Imaging floating metals and dielectric objects using electrical capacitance tomography

M Zhang, M Soleimani

Engineering Tomography Laboratory (ETL), Department of Electronic and Electrical Engineering, University of Bath, Bath, UK, Email: m.zhang@bath.ac.uk, m.soleimani@bath.ac.uk,

Abstract: Electrical capacitance tomography (ECT) is a well-established industrial process tomography technique. The application of ECT is generally limited to imaging insulating objects with permittivity contrast. Although ECT imaging for grounded conductors are studied earlier, there is not a systematic study of imaging floating metals using ECT. To broaden the application of the ECT, imaging of suspended metallic samples is studied in this paper. Placing a metallic conductor between electrodes has an effect of shortening the spacing between the electrodes, thus the capacitances are increased. This increment in capacitances can be regarded as placing a dielectric sample with higher permittivity than the reference data. An ECT image of the floating metallic samples can be reconstructed using traditional sensitivity based image reconstruction, which is in the same way as imaging dielectric permittivity. In this paper, both metallic and dielectric samples are tested, and the results show the feasibility of ECT imaging for floating metals.

Keywords: ***Electrical capacitance tomography, capacitance imaging with floating conductor***

1. Introduction

Electrical capacitance tomography (ECT) is a non-invasive method which produces tomograms of permittivity distributions by using capacitance measurements of material under test [1, 2]. Generally, ECT is considered as a suitable imaging tool for dielectric materials. In many application areas the material under test may not be a purely dielectric, but a mixture of dielectric and conductive. For low conductivity samples, such as saline water, the conductivity could decrease the ability of ECT to image the dielectric sample within the conductive background [3, 4], study of low conductivity materials in ECT is beyond scope of this paper and are presented elsewhere[5]. ECT with grounded conductors are studied earlier [6, 7].

For grounded metal in known location, Ville Rimpiläinen et al. set the boundary condition of metal to zero voltage to solve the problem of grounded conductor shaft in a mixer[7]. For the grounded metal of unknown location, Maomao Zhang et al. introduce MIT to find the location of metal and image the dielectric contrast in the remaining area in the sensor [6]. On

the other hand, for the floating metal, the conducting surface is equipotential but not in the voltage of zero. The floating metal between electrodes will increase the measured capacitance due to the reduction in spacing between the electrodes.Dixiang Chen et al. designed a security screening system using a planar capacitance sensor matrix to generate an image of an floating steel sample[8]. However the tomographic method has not been used in their screening system, the steel sample is directly imaged by the capacitance measurement of the planar sensor. In our ECT experiments, by calculating this capacitance change caused by the metallic sample in ECT, an illusion of the permittivity change is reconstructed at the location of the metallic sample. A combination of permittivity change and presence of metal sample can also be imaged using ECT. Imaging metallic samples using ECT can be potentially very useful in various areas. Possibility of metal flow imaging using ECT can be very interesting. Simultaneous reconstruction of metallic samples and dielectric samples using ECT can provide a novel solution in many non-destructive evaluation applications where there is a mixture of conductive and dielectric medium.

This paper presents imaging metallic samples and simultaneous imaging of metallic samples and dielectric samples for the first time. Analysis of metallic sample as floating and grounded conductors is shown in simple capacitance measurement enabling a better understanding of metallic imaging using ECT.

2. Methodology

2.1 Forward model

To solve the image reconstruction problem a forward problem needs to be solved. A complex value ECT forward model is needed to analyse the ECT forward problem including both conductive and dielectric materials. From Maxwell's equations, the relationship between permittivity and conductivity distribution $\varepsilon(x)$, $\sigma(x)$ and electrical potential $u(x)$ are in the following way within the region, where

$$\nabla \cdot \left(\varepsilon(x) + \frac{\sigma(x)}{j\omega} \right) \nabla u(x) = 0 \qquad (1)$$

And the boundary conditions of this problem are the electric potential $u(x)$ on different surfaces of the sensors.

$$u(x) = V \qquad on\ \Gamma_{\text{excited}} \tag{2}$$

$$u(x) = 0 \qquad on\ \Gamma_{\text{Screening}}\ and\ \Gamma_{\text{unexcited}} \tag{3}$$

where the V is the excitation voltage, $\Gamma_{excited}$ is the surface of the excited electrode, $\Gamma_{Screening}$ is the surface of the screening and $\Gamma_{unexcited}$ is the surface of the unexcited electrodes. Figure 1 shows the ECT sensor array with grounded and floating metallic inclusions.

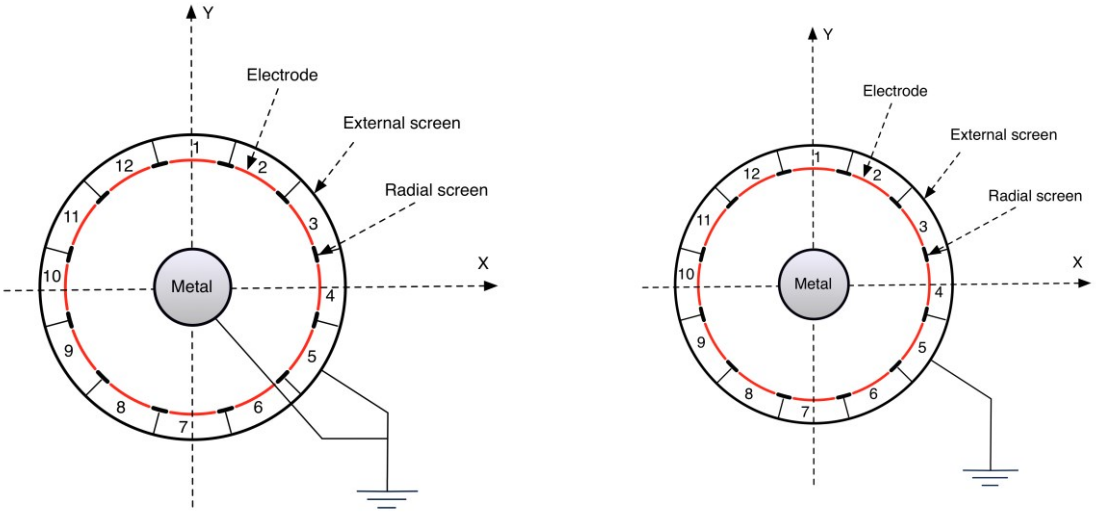

(a) (b)

Figure 1. Schematic drawings about cross section of a 12-electrode ECT sensor with (a) grounded metal or (b) floating metal

In electrical quasi-static mode, a metal sample of high conductivity performs as an equipotential body, i.e. the electrical voltage drops on the metal is negligible. When the conductor is grounded, except for that the voltage potential remains the same within the region of conductor, the value of the voltage on the conductor is zero. The boundary conditions are changed as well. For ECT forward model including dielectric and conductor, to image the dielectric components is also in need in ECT. In forward models of ECT, different settings are applied to grounded and floating conductor.

1. In the case of grounded conductor, to image the rest region excluding the conductors, the forward model of ECT can be modified since the boundary condition of the

sensing domain is changed. The grounded metal is set as an extra grounded "electrode", the voltage potential remains at zero[6]. The reference measurement is also updated: a measurement of the grounded metal standing in the sensor is used.

2. In the case of a floating conductor in ECT, the settings are different in electrostatic model or electro-quasi-static one. If the static model is used in forward problem, the region of metal is set as the same voltage but still unknown. Then the voltage will be calculated in forward model. If it is electro-quasi-static mode, every element in the mesh has a complex permittivity, which consists of both permittivity (ε) and conductivity (σ) with signal frequency (ω), i.e. $\varepsilon_{complex} = \varepsilon + \frac{\sigma}{j\omega}$. Since the frequency of exciting voltage in ECT is within radio frequency, the permittivity of metal is conductivity-dominant, i.e. the effective permittivity is an imaginary number [9].Then a big value of conductivity is assigned to the region of conductor, and normally it's the order of magnitude is about 7.

2.2 ECT – difference imageing

ECT is generally used in time difference imaging mode, calculates the capacitance changes from measurements to obtain the changes in permittivity distribution. In most commonly used ECT data, an air-filled sensor is used as the reference data with reference measurements, C_r. Then one or multiple samples are placed into the sensor, the capacitances between inter-electrodes are recorded again as sample measurements, C_s. A small perturbation of permittivity distribution brings the change between these two measurements, $\Delta C = C_s - C_r$. For ΔC_{ij}, the change of capacitance between the electrode i and j, it is expressed as below [2, 10].

$$\Delta C_{ij} = \left[\frac{\partial C_{ij}(\varepsilon)}{\partial \varepsilon_1} \quad \frac{\partial C_{ij}(\varepsilon)}{\partial \varepsilon_2} \quad \cdots \quad \frac{\partial C_{ij}(\varepsilon)}{\partial \varepsilon_n}\right]_{1*n} * \begin{bmatrix} \Delta\varepsilon_1 \\ \Delta\varepsilon_2 \\ \vdots \\ \Delta\varepsilon_n \end{bmatrix}_{n*1} \tag{4}$$

Where values of $\Delta\varepsilon_n$ is the change in permittivity distribution, and $\frac{\partial C_{ij}(\varepsilon)}{\partial \varepsilon_n}$ are the values of the sensitivity matrix. Equation (4) shows a row of sensitivity matrix. To obtain the permittivity change, the capacitance difference is calculated through the sensitivity map by inverse problem solvers, like Tikhonov or Landweber algorithms [2, 11]. In this paper a standard Tikhonov regularisation algorithm is used to calculate permittivity changes

$$\Delta\varepsilon = [S^T S + \gamma I]^{-1} S^T (C_s - C_r) \quad (5)$$

where S is the sensitivity matrix, and the level of regularisation is controlled by the factor γ, which is selected empirically in this paper.

It is worth noticing that applying ECT to image the grounded conductor, a simple model with air-reference and free space sensitivity map fails to produce suitable images. On the other hand, Hyenkyun Woo *et al* applied a tracking method for the grounded conductor [12], or a method proposed in [6] shows how MIT guided ECT can image both grounded conductor and permittivity contrasts.

2.3 Analysis of feasibility on ECT imaging grounded and floating conductor

An ideal model of a parallel-electrode capacitor is shown in Figure 2, the spacing is L and the size of electrode is A. A metallic sample with width of D is inserted between the electrodes, and the distance between the left edge of the metal and excited electrode is D_1. The permittivity of air is ε_0.

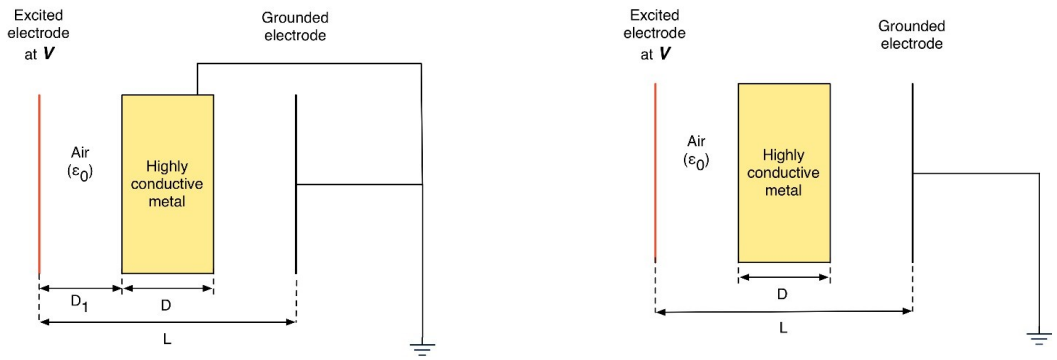

(a) (b)

Figure 2. An ideal parallel electrode model with (a) a grounded metallic sample (b) a suspended metallic sample

If the metal is grounded, as shown in Figure 2 (a), the capacitance between the electrode, $C_{grounded}$, can be expressed as:

$$C_{grounded} = \frac{\varepsilon_0 A}{D_1} \quad (6)$$

If it is suspended as Figure 2 (b), the capacitance $C_{non-grounded}$ can be expressed as below:

$$C_{non-grounded} = \frac{\varepsilon_0 A}{L - D} \tag{7}$$

In the pure dielectric model of ECT, Figure 3, the permittivity distribution is the only thing can be calculated, so the high conductivity is the region of metal cannot be computed in this way. But the conductor between two electrodes increase the capacitance measurement, this produces an illusion of higher permittivity in the sensing area.

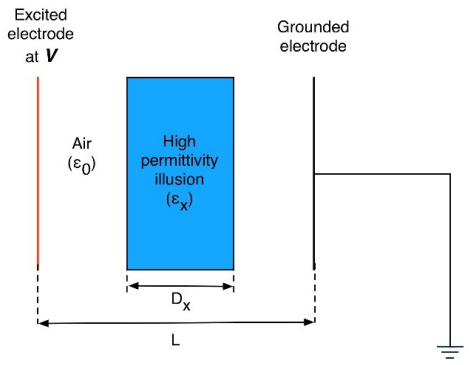

Figure 3. An equivalent dielectric illusion of an conductor

Let's set that the permittivity of the illusion is ε_x and homogeneous and the width is D_x. The capacitance for this illusion is:

$$C_{illusion} = \frac{1}{\frac{L - D_x}{\varepsilon_0 A} + \frac{D_x}{\varepsilon_x A}} \tag{8}$$

To obtain the relationship between the conductor and the illusion, we make $C_{illusion}$ equals $C_{grounded}$ and $C_{non-grounded}$ respectively.

For grounded metal: $$\frac{\varepsilon_x}{\varepsilon_0} = \frac{D_x}{D_x + D_1 - L} \tag{9}$$

For floating metal: $$\frac{\varepsilon_x}{\varepsilon_0} = \frac{D_x}{D_x - D} \tag{10}$$

If the permittivity of illusion is k times the permittivity of air, i.e. $\varepsilon_x = k * \varepsilon_0$, then relationships between the two values of width are:

For grounded metal: $$D_x = \frac{k}{k-1}(L - D_1) \tag{11}$$

For floating metal:

$$D_x = \frac{k}{k-1} D \tag{12}$$

From the equations (11) and (12), if the grounded metal is placed in ECT sensor, the size of the illusion is related to $(L - D_1)$, not to the size of the metal, D. However for the floating metal, the sizes of illusion and metal are related to each other. In fact, both $(L - D_1)$ and D are the distance shortened between parallel electrodes. So the width of illusion is proportional to shortened spacing:

$$D_x \propto D_{shortened} \tag{13}$$

Therefore, for 1-D consideration, the floating conductor performs like a dielectric sample, where ECT can be used to image this dielectric illusion. In the following sections, the experiments on imaging metallic and dielectric sample using ECT are carried out.

3. Imaging metallic and dielectric samples

A 12-electrode sensor is used to assess the ECT imaging of floating metals. In **Error! Reference source not found.** (a)The capacitance measurement unit is PTL-300E, which is a commercial product from Process Tomography Ltd[13]. The unit can collect sets of capacitance data at 100 frames per second with an effective resolution of 0.1 fF and measurement noise level better than 0.07 fF. There are two main types of the ECT measurement unit as explained in [14], an AC based system and a charge transfer system. The PTL-300E system is a charge transfer system. The metal imaging system in this paper should be possible by both these different types of ECT design method, although results here are based on charge transfer based ECT device. For more information on various ECT hardware design see [15-17].

3.1 ECT imaging of metallic samples

To show imaging of metallic samples a metallic pipe is used various locations. The metallic pipe of 32mm in diameter is used to show the feasibility of metallic sample imaging, as shown in **Error! Reference source not found.**(b). The experimental results are listed below. The directions of X-Y axes on the sensor are shown in Figure 1. The pipe is moved from the centre (0, 0) to (0, 5) cm in the sensor. The reconstruction images are in Table 1. As expected, an image of exterior surface of the conductor is possible obtained by ECT, so it might be

better to state that the ECT is capable of imaging floating metal in topographic imaging mode. It is interesting to see that the simple inversion of equation (5) primary designed for permittivity imaging is capable of producing surfaces of floating metal. Although the images of Table 1. Shows a profile of permittivity change but a transition from air to conductor is sharp change in electric field. The standard Tikhnov algorithm is introducing an artificial smoothness profile as trade off to improving the ill-posedness of the ECT inverse problem. In reality the metal will act as a shield so there is no variation inside can be detected.

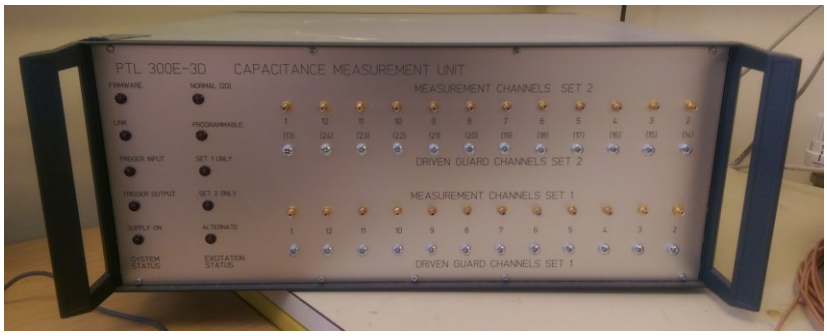

(a)

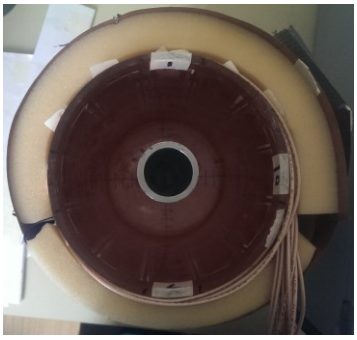

(b)

Figure 4. (a) PTL 300E capacitance measurement unit; (b) A floating metallic pipe stands in the ECT sensor.

Pipe's centre (x,y) /cm	(0,0)	(0,1)	(0,2)
ECT images	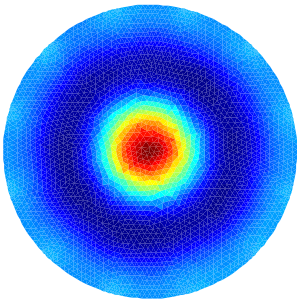	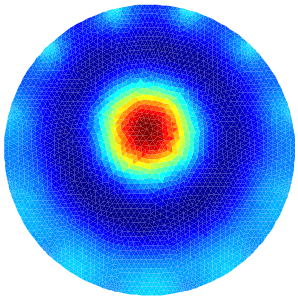	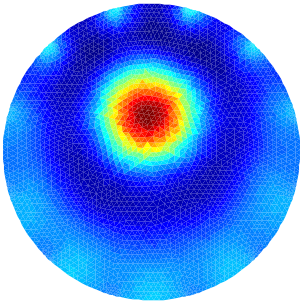
Pipe's centre (x,y) /cm	(0,3)	(0,4)	(0,5)
ECT images	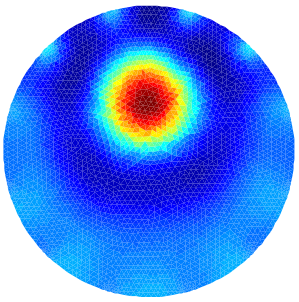	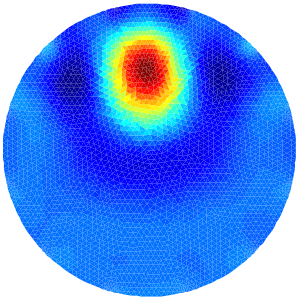	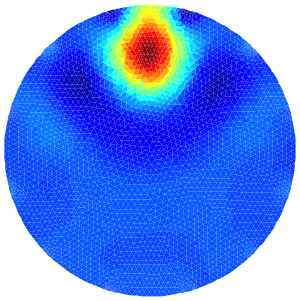

Table 1 ECT imaging of floating conductor

3.2 ECT imaging of metallic and dielectric samples

Remaining results show that simultaneous reconstruction of metallic and dielectric inclusions is examined by using a metallic pipe and wooden bars. The external diameter of the metallic pipe is 32mm. the diameter of the wood bar is 23mm. At first only one wooden sample is placed next to the pipe. In Table 2, the pipe is fixed at (0, 4) cm, and the wooden bar is moved along the Y-axis from (0,-4) to (0, 0) cm. We can see that the wood bar is the region of lighter colour, i.e. smaller reconstructed value of permittivity, while the red area stands for the metallic pipe. This is not just because of the size difference between these two samples but the different effective capacitance increment caused by them. In other words, the pipe raises more capacitance measurement than the wooden bar.

From the images, they clearly indicate that the wooden bar is approaching the metal. But when the wooden bar is close to the pipe, these two samples are merged into one on the reconstruction image. Since separating two adjacent dielectric samples is a difficult problem existing in normal ECT [10], it is also hard for a metal pipe and a wood bar.

Locations of samples' centres (x,y) / cm	Photos of experiment scenario	Reconstruction images
Metal at (0,4) Wood at (0,-4)		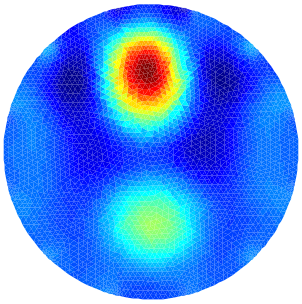
Metal at (0,4) Wood at (0,-3)		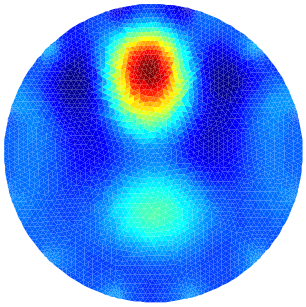
Metal at (0,4) Wood at (0,-2)		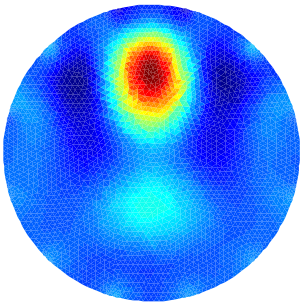
Metal at (0,4) Wood at (0,0)	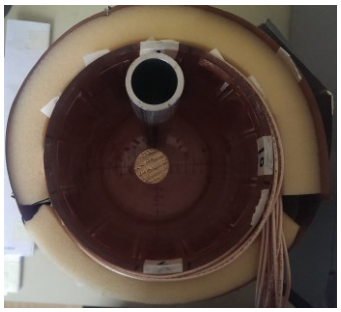	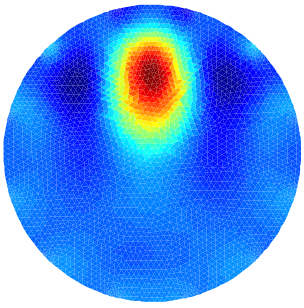

Table 2. ECT images of metal and wood.

In Table 3Error! Reference source not found., the pipe is placed at the centre. The wooden samples are standing on one or two sides of the pipe. The ECT deformed images implies the wooden samples, but still cannot separate it from metallic pipe.

Locations of samples' centre (x,y) / cm	Photos of experiment scenario	Reconstruction images
Metal (0,0) Wood (0,-4)	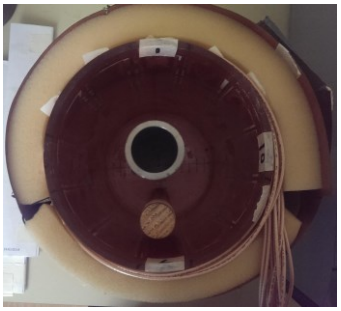	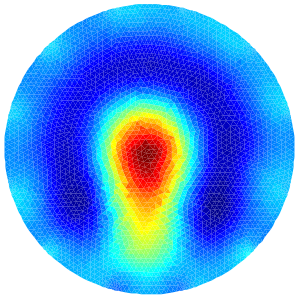
Metal (0,0) Wood 1 (0,4) Wood 2 (0,-4)		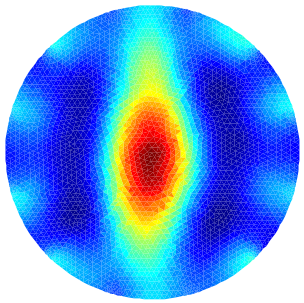

Table 3. ECT images of metal and wood.

For the cases of using the air-filled sensor as reference scenario, the ECT fails to separate the wood samples from metal. When the reference measurements are updated with the metal information, the quality of image can be improved. When the measurement of the metallic pipe standing in the air background is regarded as a reference measurement, the ECT can easily reconstruct and separate the wooden samples, as shown in **Error! Reference source not found.**. To compare the reconstruction quality, an ECT image of only two wooden samples is listed as well. The two ECT images in first two rows demonstrate a consistency between two scenarios. In third row, the result of a grounded metal with two wooden samples is presented, where the measurement of the grounded metallic pipe standing in the air background is regarded as a reference measurement. The value of the calculated permittivity distribution is in different scale from the first two rows, but also indicates the information of the two wooden bars. To detect the dielectric samples, prior information about the conductor is important. Updating the reference measurements has a big improvement in the detection and reconstruction of the dielectric components.

Reconstruction of two wooden samples with air background		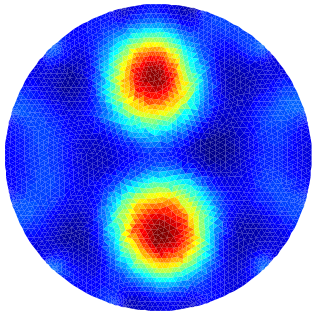
Reconstruction of two wooden samples with floating metal background		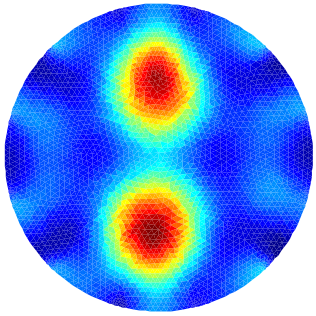
Reconstruction of two wooden samples with grounded metal background		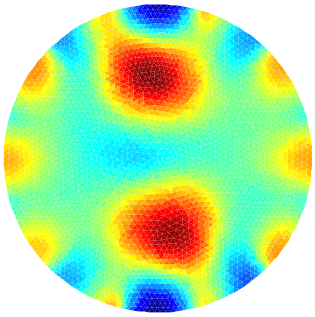

Table 4. ECT images of wooden samples with different reference measurements.

4. Conclusions

In this paper, the ability of ECT to detect a floating metallic sample or a metallic sample with dielectric samples is presented. The reason why the permittivity images of ECT can indicate the floating conductor is explained in the one-dimensional model for changes in capacitance data with floating metal as well as the meaning of the metal sample image through an algorithm primarily designed for permittivity imaging. However, ECT is not capable to distinguish the metal and dielectric in our experiments. A magnetic induction tomography (MIT) is a good choice to find the metal component, and then by combining the images from MIT and ECT, the metal and dielectric samples can be distinguished. In this paper we have demonstrated ECT is capable of imaging dielectric and metallic samples. Imaging interior of dielectric samples is possible in ECT while the ECT metal imaging only capable of imaging

of the surface of a metallic object. A combined ECT-MIT might be possible to extend the imaging of interior of metallic object, which is a subject of our future studies. The future potential of the ECT in imaging outer surface of metallic sample will be explored in future studies for metrology applications and industrial process applications such as metal flow imaging.

Reference

1. Soleimani, M., M. Vauhkonen, W. Yang, A. Peyton, B.S. Kim, and X. Ma, *Dynamic imaging in electrical capacitance tomography and electromagnetic induction tomography using a Kalman filter.* Measurement Science & Technology, 2007. **18**(11): p. 3287-3294.
2. Yang, W.Q. and L.H. Peng, *Image reconstruction algorithms for electrical capacitance tomography.* Measurement Science & Technology, 2003. **14**(1): p. R1-R13.
3. Jaworski, A.J. and G.T. Bolton, *The design of an electrical capacitance tomography sensor for use with media of high dielectric permittivity.* Measurement Science and Technology, 2000. **11**(6): p. 743.
4. Li, Y. and M. Soleimani, *Imaging conductive materials with high frequency electrical capacitance tomography.* Measurement, 2013. **46**(9): p. 3355-3361.
5. Zhang, M., L. Ma, and M. Soleimani, *Dual modality ECT-MIT multi-phase flow imaging.* Flow Measurement and Instrumentation, 2015(0).
6. Zhang, M., L. Ma, and M. Soleimani, *Magnetic induction tomography guided electrical capacitance tomography imaging with grounded conductors.* Measurement, 2014. **53**(0): p. 171-181.
7. Rimpilainen, V., S. Poutiainen, L.M. Heikkinen, T. Savolainen, M. Vauhkonen, and J. Ketolainen, *Electrical capacitance tomography as a monitoring tool for high-shear mixing and granulation.* Chemical Engineering Science, 2011. **66**(18): p. 4090-4100.
8. Dixiang, C., H. Xiaohui, and Y. Wuqiang, *Design of a security screening system with a capacitance sensor matrix operating in single-electrode mode.* Measurement Science and Technology, 2011. **22**(11): p. 114026.
9. de Fornel, P., J.M. Lourtioz, D. Pagnoux, H. Benisty, V. Berger, J.M. Gerard, D. Maystre, and A. Tchelnokov, *Photonic Crystals: Towards Nanoscale Photonic Devices*. 2008: Springer.

10. Soleimani, M. and W.R.B. Lionheart, *Nonlinear image reconstruction for electrical capacitance tomography using experimental data.* Measurement Science & Technology, 2005. **16**(10): p. 1987-1996.

11. Yang, W.Q., D.M. Spink, T.A. York, and H. McCann, *An image-reconstruction algorithm based on Landweber's iteration method for electrical-capacitance tomography.* Measurement Science & Technology, 1999. **10**(11): p. 1065-1069.

12. Hyenkyun, W., K. Sungwhan, S. Jin Keun, L. William, and W. Eung Je, *A direct tracking method for a grounded conductor inside a pipeline from capacitance measurements.* Inverse Problems, 2006. **22**(2): p. 481.

13. Byars, M. *Process Tomography Ltd Electrical Capacitance Tomography System Type PTL300E*. 9 Dec 2014 [cited 2015 5 May]; Available from: http://www.tomography.com/pdf/ptl300E.pdf.

14. Yang, W.Q., *Hardware design of electrical capacitance tomography systems.* Measurement Science & Technology, 1996. **7**(3).

15. Huang, S.M., R.G. Green, A.B. Plaskowski, and M.S. Beck, *Conductivity effects on capacitance measurements of two-component fluids using the charge transfer method.* Journal of Physics E: Scientific Instruments, 1988. **21**(6): p. 539.

16. Yang, W. and T. York, *New AC-based capacitance tomography system.* IEE Proceedings-Science, Measurement and Technology, 1999. **146**(1): p. 47-53.

17. Gonzalez-Nakazawa, A., J.C. Gamio, and W. Yang, *Transient processes and noise in a tomography system: An analytical case study.* Sensors Journal, IEEE, 2005. **5**(2): p. 321-329.